

---

## Role of fronts in the formation of Arabian Sea barrier layers during summer monsoon

Clément de Boyer Montégut<sup>1</sup>, Fabien Durand<sup>2</sup>, Romain Bourdallé-Badie<sup>3</sup>, Bruno Blanke<sup>4</sup>

<sup>1</sup> IFREMER, Centre de Brest, Laboratoire d'Océanographie Spatiale, Pointe du Diable, B.P. 70, 29280, Plouzané, France

<sup>2</sup> IRD, LEGOS, UMR5566 CNRS–CNES–IRD–UPS, 14 Avenue Edouard Belin, 31400, Toulouse, France

<sup>3</sup> Mercator Océan, 8-10 rue Hermes, Parc Technologique du Canal, 31520, Ramonville Saint-Agne, France

<sup>4</sup> Laboratoire de Physique des Océans, UMR 6523 CNRS-IFREMER-IRD-UBO, CNRS, Brest, France

Email addresses : [deboyer@ifremer.fr](mailto:deboyer@ifremer.fr) ; [fabien.durand@ird.fr](mailto:fabien.durand@ird.fr) ; [rbourdall@mercator-ocean.fr](mailto:rbourdall@mercator-ocean.fr) ; [blanke@univ-brest.fr](mailto:blanke@univ-brest.fr)

---

### Abstract:

The barrier layer (BL) — a salinity stratification embedded in the upper warm layer — is a common feature of the tropical oceans. In the northern Indian Ocean, it has the potential to significantly alter the air–sea interactions. In the present paper, we investigate the spatio-temporal structure of BL in the Arabian Sea during summer monsoon. This season is indeed a key component of the Asian climate. Based on a comprehensive dataset of Conductivity–Temperature–Depth (CTD) and Argo in situ hydrographic profiles, we find that a BL exists in the central Arabian Sea during summer. However, it is highly heterogeneous in space, and intermittent, with scales of about ~100 km or less and a couple of weeks. The BL patterns appear to be closely associated to the salinity front separating two water masses (Arabian Sea High Salinity Water in the Northern and Eastern part of the basin, fresher Bay of Bengal Water to the south and to the west). An ocean general circulation model is used to infer the formation mechanism of the BL. It appears that thick (more than 40 m) BL patterns are formed at the salinity front by subduction of the saltier water mass under the fresher one in an area of relatively uniform temperature. Those thick BL events, with variable position and timing, result in a broader envelope of thinner BL in climatological conditions. However, the individual patterns of BL are probably too much short-lived to significantly affect the monsoonal air–sea interactions.

**Keywords:** Barrier layer ; Arabian Sea ; Summer monsoon ; ARGO ; ASHSW

### 1 Introduction

---

The tropical oceans frequently present a peculiar thermohaline stratification in the upper part of the water column, known as the barrier layer (BL) (Lukas and Lindstrom 1991). It consists of a salt-stratified, stable layer embedded within the warm, upper layer of the ocean. It was termed BL because it opposes the vertical exchanges of heat between the upper mixed layer (ML) and the underlying cooler thermocline. Figure 1 exemplifies this feature in the Arabian Sea. In the absence of BL, when turbulence is high enough in the ML, cooler thermocline water is mixed and/or entrained in the ML, reducing the ML temperature. The presence of a BL completely changes this picture: the ML water can only mix with and/or entrain BL water, which is as warm or even warmer (see de Boyer Montégut et al. 2007a for a map of temperature inversions below the ML): ML water does not cool through vertical exchanges. This is known to play an important climatic role in various regions of the tropics, such as the western Pacific Ocean for El Niño initiation (Maes et al. 2005), or in the

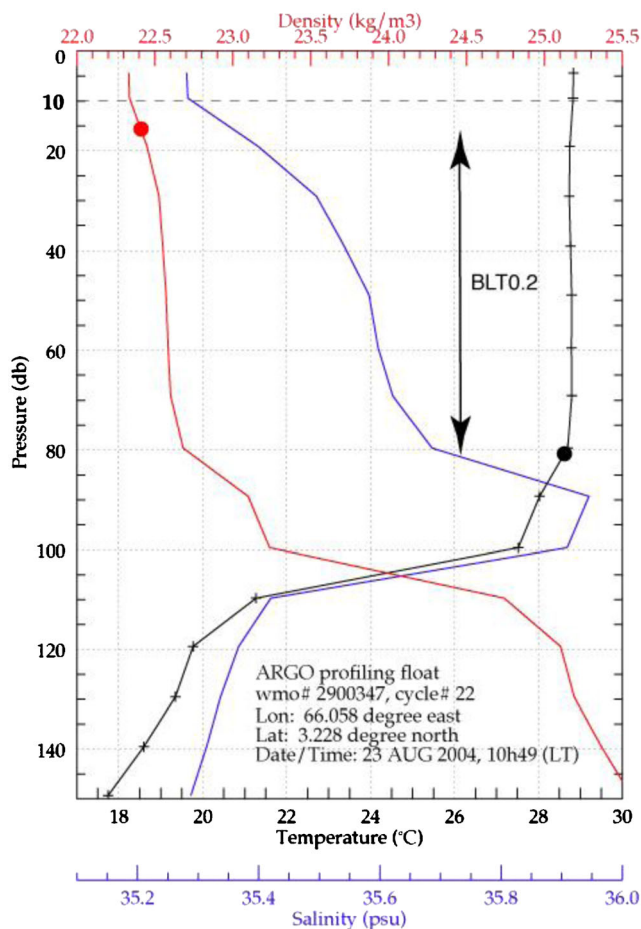


**Fig. 1** Example of a barrier layer (BL) occurrence in the upper layer of the ocean: hydrographic profiles observed by ARGO float #2900347 in the study area (66.058°E, 3.228°N) during the 2004 summer monsoon. Temperature (resp. salinity, density) is in black (resp. blue, red). The black bullet shows the depth where the temperature is 0.2 °C colder than at 10 m (T10). The red bullet shows the depth of the equivalent density increase, it represents the mixed layer depth (MLD<sub>ρ</sub>, see text). The dashed line indicates the surface reference level at 10 m depth. The BL thickness in the sense of T10-0.2 °C, named BLT0.2, is defined as the depth difference between the black and red bullets. Here, we have BLT0.2=65 m

60 South-eastern Arabian Sea for Indian monsoon onset (Masson  
61 et al. 2005). The western Pacific warm pool and the South-  
62 eastern Arabian Sea are indeed regions where the BL is a  
63 robust feature, throughout the year or in some seasons only  
64 (Mignot et al. 2007). The BL forms under various possible  
65 mechanisms. Cronin and McPhaden (2002) describe four  
66 types of processes by which a BL can form and/or grow (see  
67 their Fig. 1). First, a BL can be advected from one region to  
68 another through horizontal advection. Second, a BL can grow  
69 or decay through vertical stretching of the water column. The  
70 two mechanisms both require a pre-existing BL to occur and  
71 will not create “new” BL conditions by themselves. Third,  
72 rainfall can cause a new BL to form between the base of the  
73 newly formed fresh lens and the top of the thermocline. Last,

the “tilting” mechanism forms a barrier layer when a vertically  
sheared horizontal flow advects a horizontal salinity gradient  
within the isothermal surface layer. This causes near-vertical  
salinity contours to tilt along the horizontal, thus generating a  
shallow halocline above the top of the thermocline. An important  
point raised by Cronin and McPhaden (2002) is that “when  
analysing the formation of barrier layers, one must consider not  
only processes governing salinity stratification, but also how they  
occur without generating a corresponding temperature stratifica-  
tion.” This is especially true for the tilting mechanism, which  
requires both a shear component in the horizontal direction  
across the salinity horizontal gradient and a relatively smaller  
temperature horizontal gradient (as regards to density variations)  
in the same direction.

The tilting mechanism appears as a singular process, in that  
it does not require the pre-existence of a BL, nor any atmo-  
spheric freshwater supply. Durand et al. (2007) demonstrated  
that the latter mechanism is basically responsible for the thick  
BL observed in the South-eastern Arabian Sea in winter. More  
controversial is the BL reported by Rao and Sivakumar (2003;  
henceforth RS03) and by Thadathil et al. (2008; henceforth  
T08) in the South Central Arabian Sea (SCAS) during summer  
monsoon. These authors suggested that a thick (20–60 m)  
BL forms there in June, and survives until September, over an  
extended area. To explain its formation, T08 proposed a  
mechanism amounting to tilting, consisting of a large-scale  
foliation of low-salinity water of equatorial origin at the sur-  
face, blanketing Arabian Sea High Salinity Water (ASHSW;  
Prasanna Kumar and Prasad 1999; Prasad and Ikeda 2002)  
at subsurface. This conclusion stands in contrast with that of  
Mignot et al. (2009; henceforth M09) and of Agarwal et al.  
(2012; henceforth A12). Indeed, based on different observa-  
tional datasets and/or gridding methodologies, these authors  
basically showed that limited BL patterns, from 5 to 20 m  
thick, are observed in the SCAS in summer. The area is known  
to present limited precipitation during summer monsoon (typi-  
cally less than 200 mm over June–September to the west of  
65°E; Hoyos and Webster 2007), which makes unlikely a  
local formation of the BL by the “rainfall” mechanism of  
Cronin and McPhaden (2002). It rather presents a deep ML  
during this season, owing to the vigorous Findlater jet that  
blows northeastward from June through October (de Boyer  
Montégut et al. 2007b). Such an energetic turbulent mixing  
does not favour a consistent, thick BL, lasting several months.  
M09 provided a quantification of the patchiness of the BL  
regarding some given space and time scales, under the form of  
a “porosity” parameter, called barrier layer porosity (BLP).  
For a given grid box (e.g., 2°×2°, 1 month), this is defined as  
the ratio of the number of non-existing or insignificant BL  
thickness (BLT) over the total number of profiles in the box.  
Thus, assuming we have enough profiles in the box and they

126 are distributed rather homogeneously (see M09 for de-  
 127 tails), it approximates the probability that the water  
 128 column does not present any BL in a given spatio-  
 129 temporal box. In our example ( $2^\circ \times 2^\circ$ , 1 month grid  
 130 box), a porosity of 50 % is consistent with a BL lasting  
 131 only half of the month or occurring only over half of  
 132 the grid cell, or a mix of the two. Interestingly, their  
 133 results show that the BL appearing in the SCAS during  
 134 summer monsoon has a porosity of about 50 % (ranging  
 135 from 25 % to 75 % for  $2^\circ \times 2^\circ$ , monthly grid boxes).  
 136 Hence, it may not be considered as a robust and durable  
 137 feature regarding space-time scales of 1 month and  
 138 200 km.

139 The present study basically aims at reconciling the four  
 140 contradictory studies of RS03, T08 on one hand, and M09 and  
 141 A12 on the other hand. Specifically, we revisit the following  
 142 issues: What is the observed seasonal evolution of the BL in  
 143 the SCAS? What is its spatial structure? How does it vary  
 144 from year to year? What is the mechanism that forms it? Has it  
 145 a sufficient time and space extension to play any climatic role?  
 146 To do so, we make use of in situ observations and of an ocean  
 147 general circulation model.

148 The paper is organized as follows. Section 2 presents the  
 149 dataset and the numerical model. Sections 3 and 4 quantita-  
 150 tively detail the observed and modeled BL, respectively.  
 151 Section 5 investigates its formation mechanism. Section 6  
 152 concludes the study.

153 **2 Data and methods**

154 **2.1 In situ data**

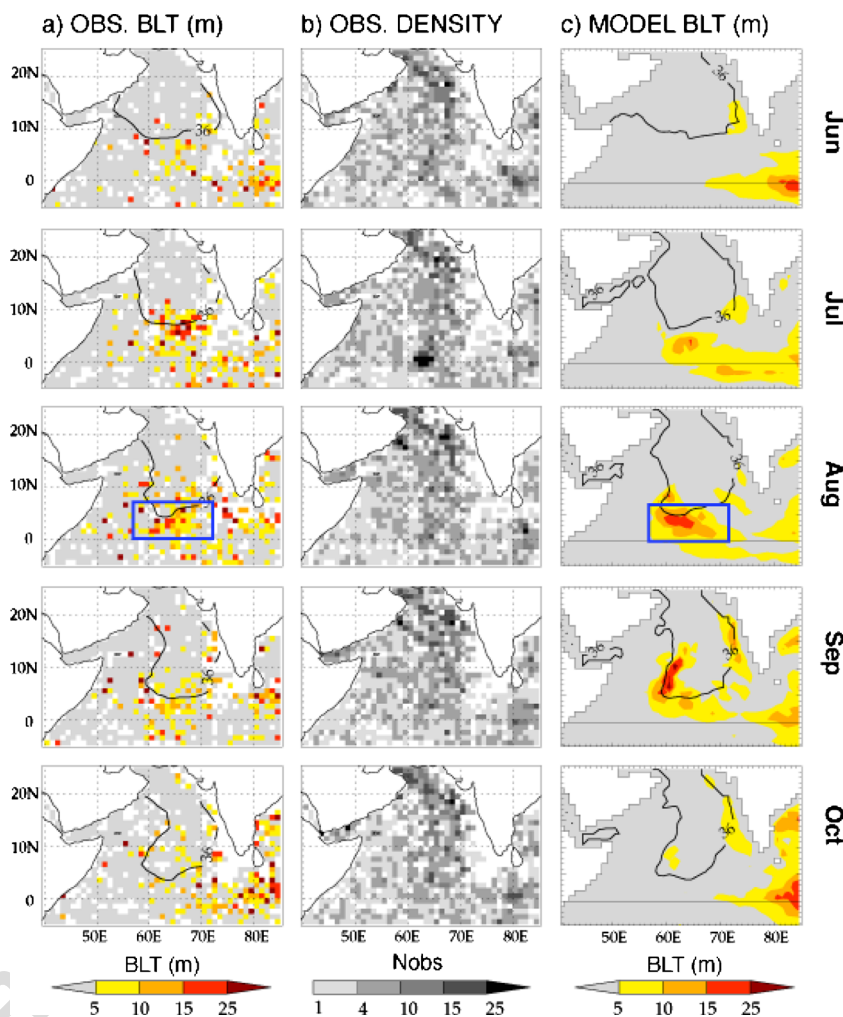
155 In the present study, we use in situ profiles of temperature and  
 156 salinity measurements coming from the Conductivity–  
 157 Temperature–Depth (CTD) profiles of the World Ocean  
 158 Database 2009 (WOD09), and from the profiling floats of  
 159 the Argo program. WOD09 covers the period 1974 to 2008  
 160 quite irregularly with more data around 1980 and in the 1990s.  
 161 Argo floats data span the 2002–2012 period. For our study  
 162 area, i.e., the Arabian Sea ( $40^\circ\text{E}–85^\circ\text{E}$ ,  $5^\circ\text{S}–25^\circ\text{N}$ ), it makes a  
 163 total of 41,496 pairs of T/S profiles (36,568 Argo profiles and  
 164 4,928 CTD profiles). Those data went through basic checks  
 165 (depth and density inversion, outlier range, gradient check)  
 166 and only Argo measurements with quality flags 1 (“good  
 167 data”) or 2 (“probably good data”) were kept here. CTD  
 168 vertical resolution is of order 2 m while Argo profiles vertical  
 169 resolution is about 10 m or less in the upper 100 m. Regarding  
 170 the latter, a BLT less than 5 m should thus be viewed with  
 171 caution and considered as a situation where no significant BL  
 172 exists (see grey shading in Fig. 2).

Our BLT criterion is based on a  $0.2^\circ\text{C}$  threshold, following  
 de Boyer Montégut et al. (2007a). The BLT is computed as  
 the difference between the top of the thermocline depth  
 (TTD; defined as the depth where temperature decreases  
 by  $0.2^\circ\text{C}$  compared to temperature at 10 m depth), and  
 the ML depth in density, using the associated variable  
 density criterion (MLD $\rho$ ; defined as the depth where  
 density increases by an amount corresponding to a  
 $0.2^\circ\text{C}$  temperature decrease). The BLT is computed from  
 individual profiles as in de Boyer Montégut et al. (2004), and  
 we will only present here monthly binned fields at  $1^\circ$  resolu-  
 tion. The binning on the regular grid was done by picking the  
 median BLT value of all individual observed profiles available  
 in each grid cell.

2.2 Model

The model used in this work is the ORCA025 version of the  
 NEMO (Nucleus for European Modelling of the Ocean) ocean  
 general circulation model (Madec 2008). The model solves  
 the primitive equations on an Arakawa (1966) C-grid over the  
 global ocean, with  $0.25^\circ$  horizontal resolution and 50 vertical  
 levels on a z-grid. The vertical resolution varies with depth  
 (viz. 1 m at the surface, 10 m at 50 m, 20 m at 100 m) in order  
 to satisfactorily simulate the ML dynamics. The vertical  
 physics is based on a prognostic equation for the tur-  
 bulent kinetic energy (Blanke and Delecluse 1993). The  
 lateral diffusion is computed along isopycnal levels,  
 with a Laplacian parameterization ( $K_h=300\text{ m}^2\text{ s}^{-1}$ ).  
 The lateral viscosity is computed along horizontal levels  
 with a bi-Laplacian operator ( $A_h=-1.5\cdot 10^{11}\text{ m}^4\text{ s}^{-2}$ ). Viscosity  
 is enhanced within  $[2.5^\circ\text{S}, 2.5^\circ\text{N}]$  by adding a Laplacian  
 parameterization with the viscosity coefficient reaching  
 $200\text{ m}^2\text{ s}^{-1}$  at the equator. The model starts from a motionless  
 state on 1 January 1999 with World Ocean Atlas (WOA;  
 Locarnini et al. 2006; Antonov et al. 2006) temperature and  
 salinity fields and runs until end of 2006. In order to get rid of  
 the model spinup phase, we consider the simulation over the  
 2002–2006 period only. The atmospheric boundary condi-  
 tions consist of surface fluxes of momentum, heat, and fresh-  
 water. The momentum and precipitation fluxes are prescribed;  
 all other fluxes (heat and evaporation) are diagnosed from  
 specified atmospheric variables through the CLIO (Coupled  
 Large-scale Ice–Ocean model) bulk formulae (Goosse et al.  
 2001). All atmospheric fields (including momentum and pre-  
 cipitation) are daily means computed from the ECMWF 6-  
 hourly operational analysis (<http://www.ecmwf.int/products/forecasts/guide/>). The model sea surface salinity (SSS) is  
 weakly restored to WOA climatology to prevent any long-  
 term drift of SSS. The large-scale component of the precipi-  
 tation flux is nudged towards Global Precipitation  
 Climatology Project (GPCP; see <http://precip.gsfc.nasa.gov/>)

**Fig. 2** **a** Monthly climatology of the observed BLT for the summer monsoon season. The month is indicated on the *right-hand side*. The frame in *blue* delimits the South Central Arabian Sea (SCAS) domain, used subsequently in this study. The 36 psu isoline at 70 m depth from Roemmich and Gilson dataset (2009), corresponding to the limit of the ASHSW (Prasad and Ikeda 2002), is also shown. **b** Corresponding distribution of the number of profiles per  $1^\circ \times 1^\circ$  mesh box. **c** Same as **a** for the model simulation, and at 78 m depth for the 36 psu isoline



223 monthly data within 30°N–30°S. The model simulation is  
 224 stored as 3-day running means. The model set-up is very  
 225 similar to the one used in Durand et al. (2013). It was found  
 226 to reproduce satisfactorily the seasonal cycle of temperature,  
 227 salinity and currents in the Northern Indian Ocean (not shown;  
 228 see Durand et al. (2013) and references therein for a complete  
 229 validation of the model run). A specific validation of the seasonal cycle of the model SSS is provided as supplementary material (see Fig. S1). The BLT in the model outputs is based on the same criterion as for the observations. We will specifically validate this parameter in Section 4.

235 **3 Observed structure of the BLT**

236 **3.1 Climatology**

237 Figure 2a presents the monthly climatology of BLT from  
 238 observations, from June to October. The BL builds up in the

SCAS in June, peaks in July–August and decays after-  
 wards. It disappears by October. Data coverage gives a  
 good confidence in the observed evolution (Fig. 2b).  
 The BLT barely reaches 25 m locally in July–September,  
 and only for a few grid cells. No broad, consistent area  
 of large BLT appears (unlike what was seen for exam-  
 ple in the South-eastern Arabian Sea in winter by  
 Durand et al. 2007). To a certain extent, the isolated  
 patches of large BLT that occur in the observations are  
 associated with the presence of the subsurface 36 psu  
 isohaline, which is known to be a good proxy for the  
 limit of the ASHSW at about 70 m depth (Prasad and  
 Ikeda 2002).

The average BLP in the observations at 2° resolution  
 in August over the SCAS box (57°E–72°E; 0–7°N) is  
 50 %. This indicates that space and lifetime of the BL  
 are of order 15 days and/or 100 km or less. For compar-  
 ison, the South-eastern Arabian Sea in January shows a BLP  
 lower than 10 % over an area of more than 5°×5°, thus  
 showing a large region of permanent BL there.



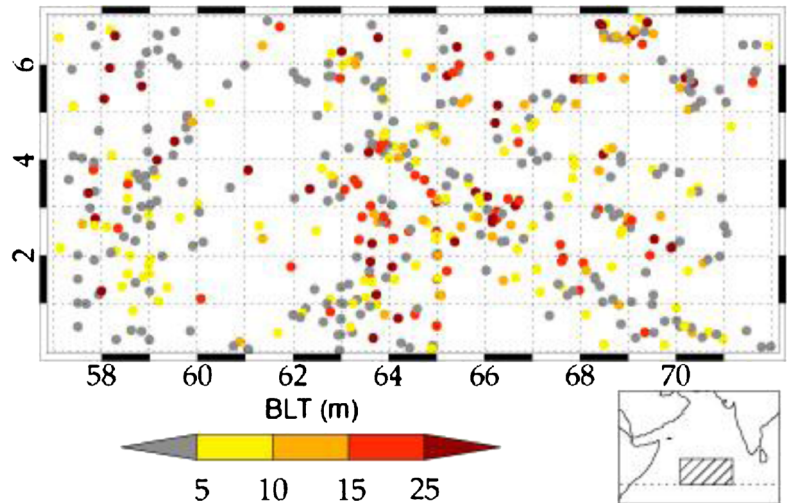
259 3.2 Variability of the BLT

260 Figure 3 shows the detailed locations of individual (profile-  
261 wise) BLTs in observations for August in the SCAS, along

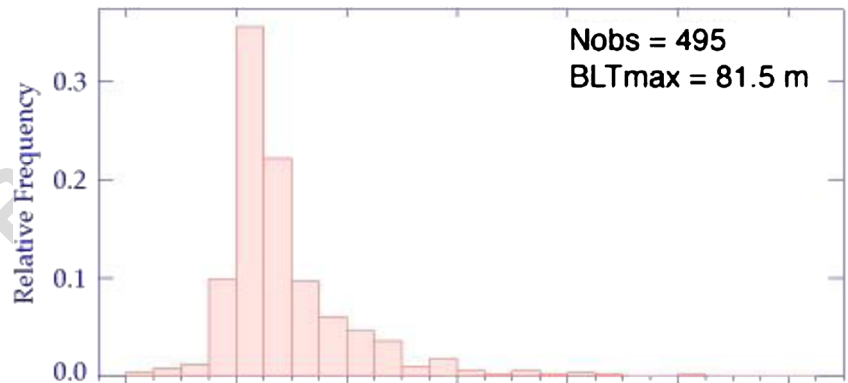
with their distribution. The BL appears to be very patchy, with 262  
the occurrence of BL-free situations (grey bullets in Fig. 3) all 263  
over the area. The BLT distribution is skewed, with a maxi- 264  
mum peak below 5 m. Those results echo the above- 265

**Fig. 3** **a** Map of observed BLT recorded for all the individual profiles falling in August over the SCAS domain. The full domain is shown as an insert. **b** Distribution of BLTs in August in the SCAS domain for the observations. **c** Same as **b** for the model

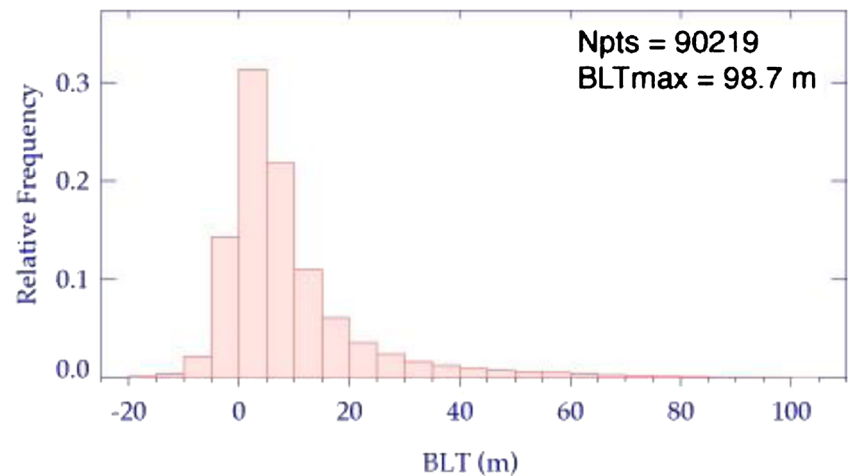
**a) BLT from OBSERVATIONS (T-S profiles) in August**



**b) Distribution of BLT from OBSERVATIONS in August**



**c) Distribution of BLT from MODEL in August**



266 mentioned high BL porosity over our area (about 50 %).  
 267 Consistently, half the distribution of BLT is below 5 m.  
 268 BLTs reach values in excess of 50–60 m on some occasions  
 269 but these events are quite rare.

270 **4 Barrier layer simulated by the model**

271 4.1 Climatology

272 Figure 2c presents the model monthly climatology of BLT  
 273 computed over 2002–2006, with the resolution of the model  
 274 downgraded to 1° to be consistent with the observational grid.  
 275 The first point to notice is that the model simulates a BL in the  
 276 Arabian Sea during the summer season, consistently with the  
 277 observations. The BLT maximum modeled in the SCAS is  
 278 located satisfactorily. Its seasonal evolution is also in line with  
 279 the observations, with an initiation in June, a maximum  
 280 reached in August, followed by a decay through October.  
 281 Co-occurrence of thick BLT areas and of the ASHSW limit  
 282 at subsurface (78 m depth) is also seen in the model. At this  
 283 resolution (1°), the BLT hardly reaches 25 m on few occasions,  
 284 just like in the observed field. When considering the  
 285 native 0.25° resolution of the model, BLP also amounts to  
 286 about 50 % over the SCAS. One exception is the small area of  
 287 200 km width centred on 64°E–2°N (maximum BLT in  
 288 August) that shows BLP lower than 10 %, revealing a quasi-  
 289 permanent BL there in the model. On average, significant BL  
 290 events (in the sense: thicker than 5 m and thicker than 10 % of  
 291 the TTD; see M09) occur twice in August, and last about  
 292 10 days each. Since the BLP is 50 % on the 0.25° grid, the  
 293 order of magnitude for the BL space scale is about 20 km,  
 294 using factors 2/3 in time (for 20 days of BL over the month,  
 295 see above) and thus 3/4 in space. One must keep in mind that  
 296 the spatial scales resolved by the model are very distinct from  
 297 that resolved by the observed climatology. This is clearly seen  
 298 in the remnant meso-scale patterns that show up in the model  
 299 climatology, but cannot be resolved by the observational grid  
 300 of 1°×1°.

301 4.2 Year-to-year variability of the modeled BLT

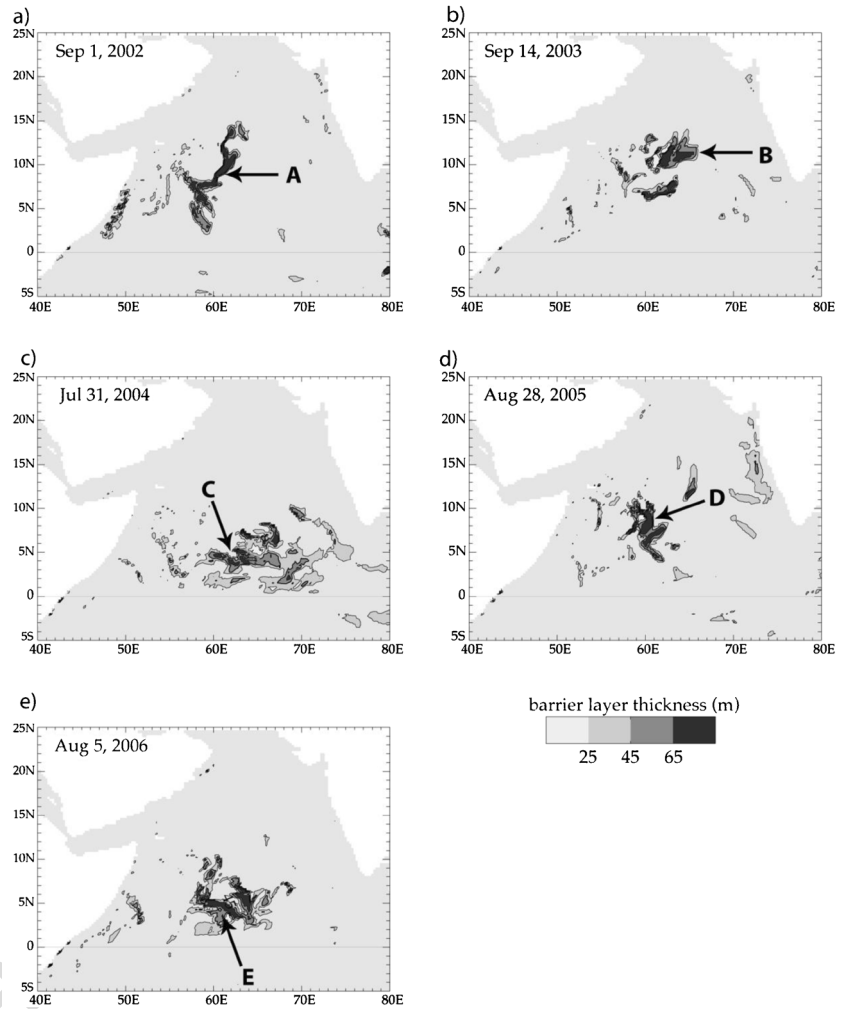
302 Figure 3c shows the distribution of modeled BLT in August.  
 303 Just like in the observed field, the distribution is skewed, with  
 304 very limited number of BL events thicker than 50–60 m.  
 305 Figure 4 presents the instantaneous structure of the BL simu-  
 306 lated by the model at the exact date when BLT reaches its  
 307 annual maximum in the Arabian Sea, during summer (from  
 308 June to October), for each year from 2002 to 2006. Note that  
 309 the timing of this maximum shows some year-to-year vari-  
 310 ability, from late July (in 2004) to mid September (in 2003). It  
 311 is obvious that the BL in the SCAS never appears as an  
 312 organized large-scale feature. Rather, it takes the form of

313 elongated patterns, reminiscent of mesoscale fronts. The typ- 313  
 314 ical width of a given feature is about 100 km, with a typical 314  
 315 length of a few hundreds of km. The orientation of the patterns 315  
 316 is extremely variable, from north–south (on 1 September 316  
 317 2002) to east–west (on 31 July 2004). The simulated BLT is 317  
 318 very large (in excess of 65 m in the core of the individual 318  
 319 patterns) but confined in space. The gradients of BLT are thus 319  
 320 extremely marked, over scales close to the model grid spacing 320  
 321 (0.25°). On each snapshot, one can typically see two patterns 321  
 322 of thick BL, one close to the other. This stands in contrast with 322  
 323 the smoother pattern seen on the monthly climatological evolu- 323  
 324 tion (Fig. 2c) and suggests that the climatological BL area 324  
 325 seen in SCAS in summer should actually be considered as the 325  
 326 geographical envelope of thicker, intermittent features, appar- 326  
 327 ently distributed randomly within the SCAS. 327

328 **5 Barrier-layer formation process**

329 Figure 5 presents the instantaneous salinity field simulated at 329  
 330 78 m depth on the same dates as the occurrence of the yearly 330  
 331 maximum BLT (shown in Fig. 4), for each year from 2002 to 331  
 332 2006. This depth was chosen because it corresponds to the 332  
 333 typical depth of the core of the BL. As we already saw in the 333  
 334 validation of the model (Section 2), it reproduces satisfactorily 334  
 335 the two water masses that are known to co-exist in the Arabian 335  
 336 Sea, with the ASHSW (salinity in excess of 36.2 psu; Prasad 336  
 337 and Ikeda 2002) in the north-eastern quarter of the basin and 337  
 338 the Bay of Bengal Water (BBW; salinity inferior to 35.8 psu; 338  
 339 Tomczak 1999) occupying the rest of the basin. A frontal 339  
 340 salinity zone, typically centred on 35.8–36.2 psu, separates 340  
 341 the two water masses. This stands in very good agreement 341  
 342 with the observed climatologies reported by Prasanna Kumar 342  
 343 and Prasad (1999) or Chatterjee et al. (2012) (Fig. S1). 343  
 344 Figure 5 also displays the positions of the grid points present- 344  
 345 ing an extremely thick BL at the time considered for plotting. 345  
 346 These grid points are objectively defined by a threshold in 346  
 347 BLT, conveniently chosen for each snapshot in order to isolate 347  
 348 a few dozens of points (for a reason explained in the next 348  
 349 paragraph). The value of the threshold as well as the resulting 349  
 350 number of grid points is provided in Table 1. Interestingly, the 350  
 351 patches of thick BL are concentrated in the frontal area and, in 351  
 352 each of the presented snapshots, the pattern of thickest BL 352  
 353 stretches exactly along an iso-haline featuring the salinity 353  
 354 front. The three-dimensional structure of these patterns is 354  
 355 investigated in Fig. 6. It presents vertical sections of temper- 355  
 356 ature and salinity in the east–west (years 2002, 2003 and 356  
 357 2005) or north–south (years 2004 and 2006) direction. They 357  
 358 are defined so as to cut through the salinity front in each area 358  
 359 of maximal BLT. The frontal salinity structure allows to 359  
 360 delineate the two water masses already introduced in the upper 360  
 361 100 m, with ASHSW corresponding to salinities in excess of 361  
 362 36.2 psu confined in the eastern (2002, 2003, 2005) or in the 362

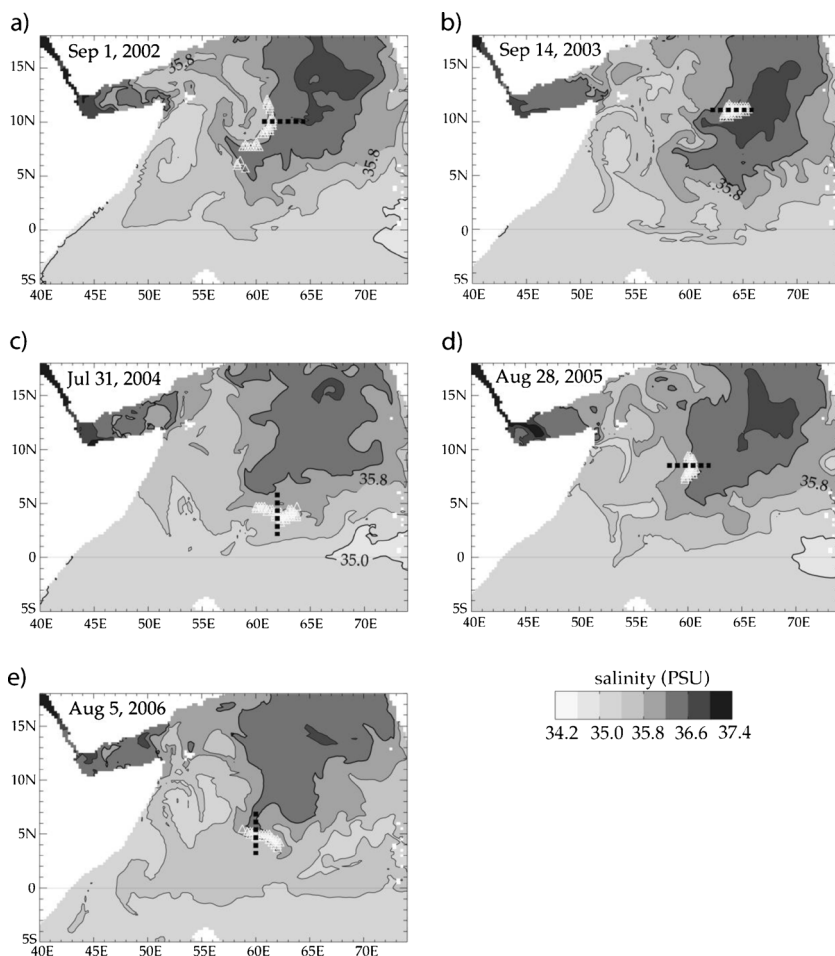
**Fig. 4** BLT simulated by the model on selected dates, as indicated on each frame. The patterns indicated by *arrows* will be studied in detail. Isocontours are every 20 m



363 northern (2003, 2006) part of each section, and BBW on the  
 364 other side. The salinity gradient is associated with a tempera-  
 365 ture gradient only for the 2002 and 2003 events. At the exact  
 366 position of the maximum BLT, the profiles of temperature and  
 367 salinity show that the model simulates a typical increase in  
 368 salinity of about 0.15–0.2 psu between the surface and the core  
 369 of the BL (in 2002, 2003, 2004 and 2005), reaching an extreme  
 370 0.5 psu in 2006. The BL typically lies between 20–50 and 100–  
 371 130 m. A weak vertical temperature gradient exists from the  
 372 surface down to the bottom of the BL. From these vertical  
 373 sections, it becomes clear that the BL is associated with sub-  
 374 surface inflow of ASHSW, leaking below the BBW lying at the  
 375 surface. Strikingly, the foliation of ASHSW below BBW occurs  
 376 typically over a band 100–300 km wide only. In a nutshell,  
 377 the model simulates small-scale BL patterns, intimately linked  
 378 with the salinity front. This is consistent with what has been  
 379 seen in the observations in Section 3. The detailed structure of  
 380 the modeled BL is hard to validate extensively, given the  
 381 limited space-time coverage of the available observations.  
 382 However, on some occasions in situ data allow to confirm the  
 383 picture inferred from the model outputs (see Fig. S2).

To understand more clearly the three-dimensional circula-  
 tion leading to the formation of these BL structures in the  
 SCAS, we make use of an offline Lagrangian trajectory analysis  
 tool (Blanke and Raynaud 1997). This tool allows tracing  
 the pathways of a given water mass, and provides its thermal  
 and haline properties along the diagnosed streamlines (Blanke  
 et al. 1999). We adopt an approach very similar to Durand  
 et al. (2007) by tracing backward in time the pathway and  
 salinity of the water mass eventually found in the core of each  
 of the five BL patterns discussed in the previous paragraph.  
 We do this by initializing Lagrangian synthetic particles at  
 every grid point constituting the area of maximum BLT (the  
 positions of the grid points are shown by triangles in Fig. 5  
 and their number is given in Table 1). We then trace their  
 trajectories backward in time by integrating the 3-day model  
 currents from the date of the maximum BLT (indicated in  
 Figs. 4, 5, and 6). As expected from the time considerations  
 given in Section 4.1, we found that for all the events, a 55-day  
 integration is long enough to cover the BL formation phase.  
 Figure 7 presents the result of the Lagrangian tracing, with the  
 age, depth and salinity of the particles plotted along the

**Fig. 5** Modeled salinity at 78 m depth on the same dates as for Fig. 4. *White triangles* show the locations where the BLT exceeds the threshold specified in Table 1. The *thick dashed lines* locate the sections presented in Fig. 6. Isocontours are every 0.4 psu



streamlines. For every BL event from 2002 to 2006, the particles predominantly follow a southward route originating in the northwestern Arabian Sea. This roughly corresponds to the orientation of the salinity front shown in Fig. 5, for each year. Some of the particle batches (2002, 2004, 2005) exhibit an undulating trajectory, in line with the known presence of large anticyclonic eddies (Great Whirl, Socotra Gyre) in this part of the basin during summer monsoon and centred to the west of the region we analyse (e.g., Wirth et al. 2002; Esenkov et al. 2003). Almost all batches experience downwelling along their trajectory, from an initial depth of about 10–30 m to a final depth of about 60 m when they end up in the core of the BL. The only exception is the 2003 batch that experiences a

quasi-horizontal displacement (i.e., with little depth variability along streamlines). In general, the salinity of the particles does not vary much along streamlines, in accordance with circulation pathways broadly parallel to the direction of the salinity front. Everything above suggests that the BL formation mechanism corresponds to the “tilting” defined by Cronin and McPhaden (2002), but with a slight difference: all (but one) batches of particles show unambiguous sign of a subduction in the period preceding the BL buildup. ASHSW flows south-eastward (and downward), and finally gets blanketed locally by BBW to form the BL at the frontal zone. In a manner similar to Lagrangian tracing of the BL water mass, we also investigated the origin of the ML water overlying the BL for all the events, in the same way as Durand et al. (2007); we do not detail the results here for the sake of conciseness. We found that the ML water prominently originates from the western Arabian Sea (either in the Somali Current or further offshore in the interior Arabian Sea) and flows westward before reaching the frontal area. Therefore, the BL formation process resembles the one evidenced in the frontal zone of the western equatorial Pacific Ocean by Vialard and Delecluse (1998) with a similar model. Here, however, the movement of the water mass

t1.1 **Table 1** Threshold in BLT chosen to define the maximum BLT area plotted for each year in Fig. 5

t1.2	Year	2002	2003	2004	2005	2006
t1.3	BLT threshold	80 m	60 m	75 m	80 m	80 m
t1.4	Number of grid points	34	36	41	24	30

The number of model grid points passing the threshold criterion is also indicated

418  
419  
420  
421  
422  
423  
424  
425  
426  
427  
428  
429  
430  
431  
432  
433  
434  
435  
436  
437  
438  
439  
440



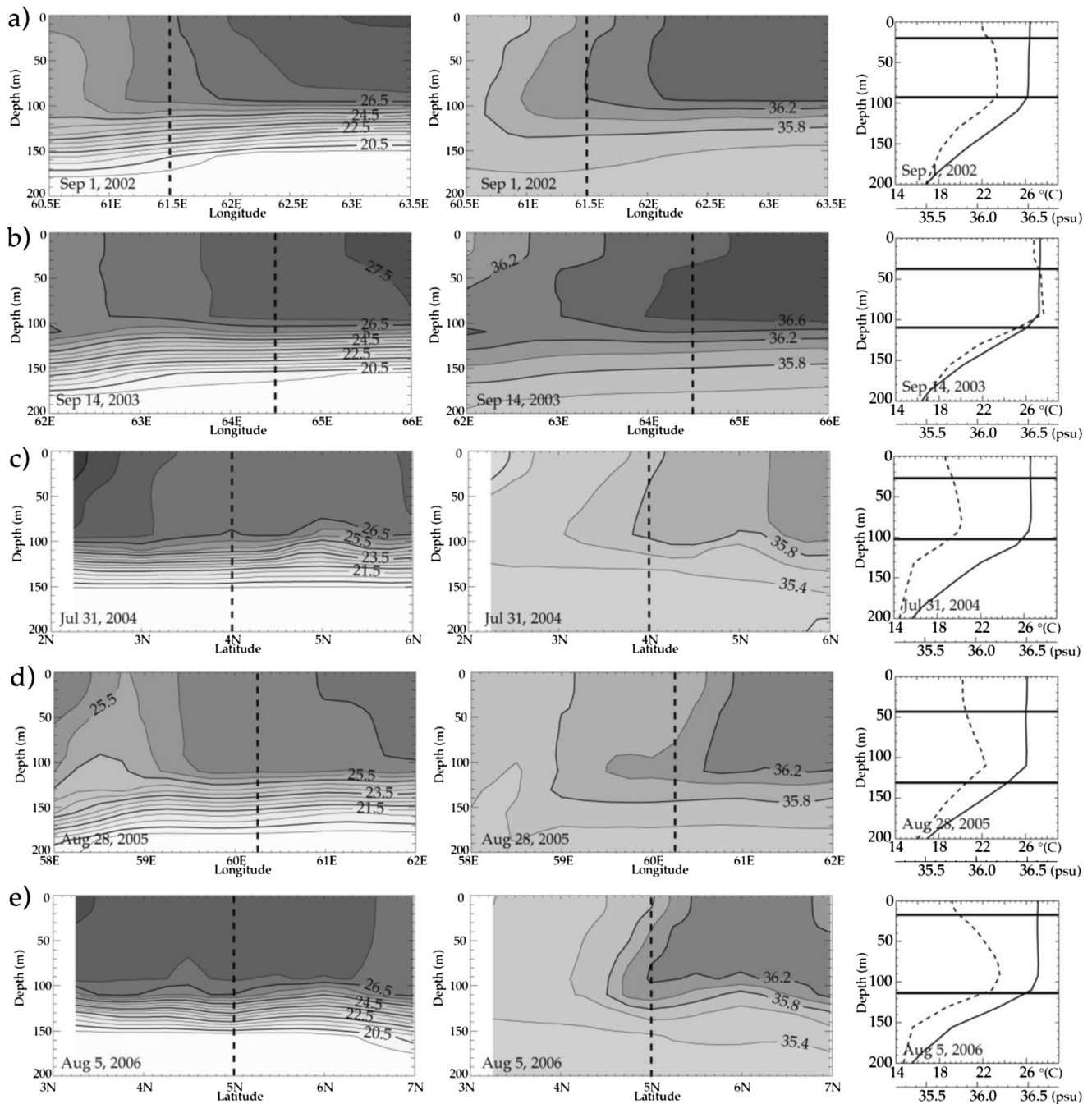
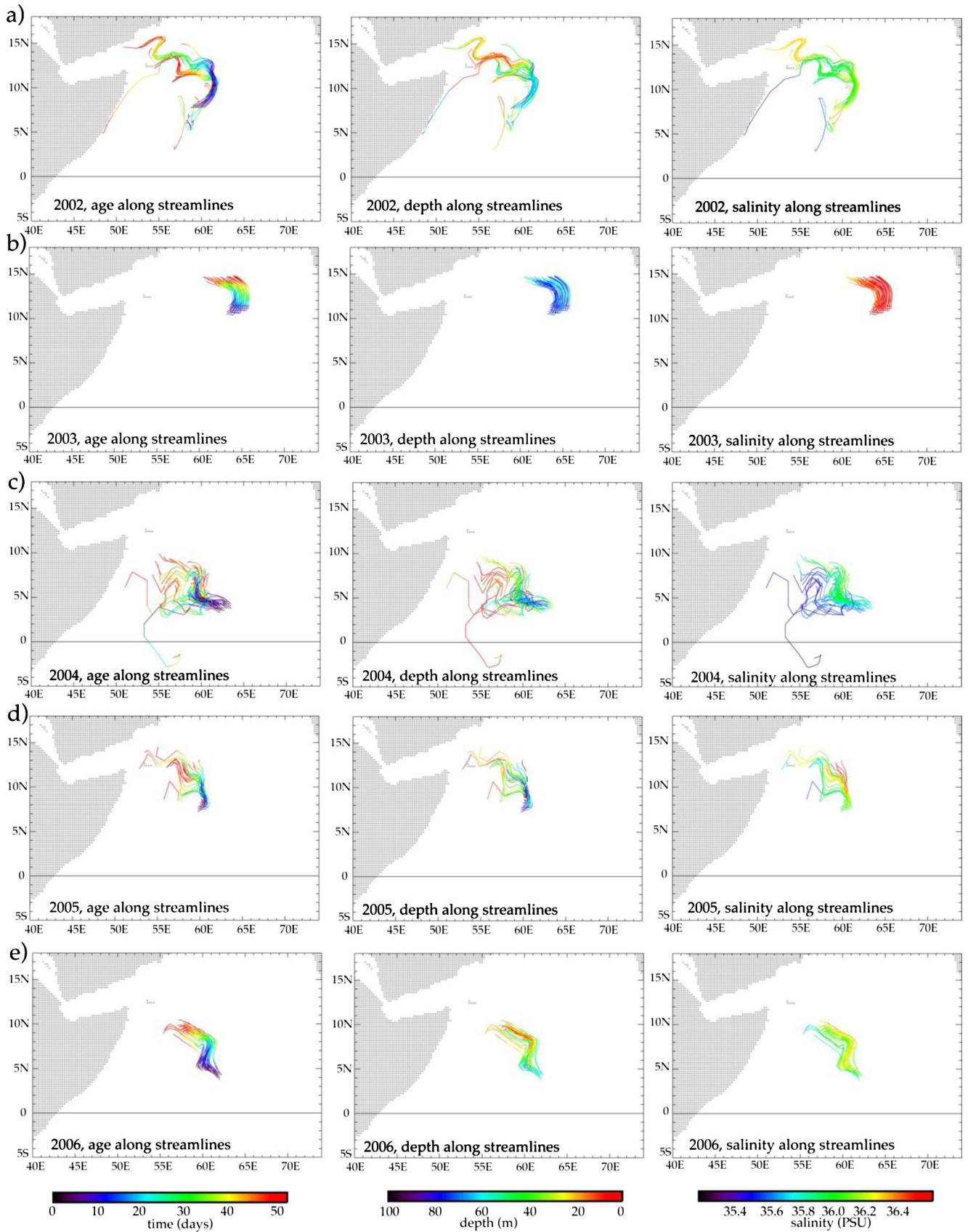


**Fig. 6** *Left column:* vertical sections of modeled temperature along the sections shown in Fig. 5 and for the same five dates (panels a to e; years 2002 to 2006). The contour interval is 0.5 °C. *Middle column:* same as left column, but for salinity and with a 0.2 psu contour interval. *Right column:* temperature (*full line*) and salinity (*dashes*) profiles extracted at the

position shown by the *vertical dashed lines* on the *left and middle columns*, located in the core of the BL. The *two horizontal lines* show the depth of the mixed layer (MLDp) and the depth of the top of the thermocline (TTD, defined following the criteria mentioned in Section 2). The BL is thus seen as the layer comprised between these two lines

441 whose fate is the core of the BL occurs predominantly  
 442 in a direction parallel to the salinity front, whereas the  
 443 BL analysed by Vialard and Delecluse (1998) was formed  
 444 by subduction in the cross-frontal direction. We applied the  
 445 same Lagrangian analysis to the three thickest BL patterns  
 446 simulated by the model each year, from 2002 to 2006 (thus  
 447 amounting to 15 patterns; not shown). This extended

448 diagnosis essentially confirms what is seen from the five  
 449 major patterns thoroughly analysed: most of the BL patterns  
 450 are formed by tilting through subduction of ASHSW below  
 451 BBW, in a region of small horizontal extent centred on the  
 452 salinity front. On a few occasions, the BL is formed by  
 453 pure tilting mechanism, without any vertical migration  
 454 of the water masses.



◀ **Fig. 7** *Left column:* age of Lagrangian particles along model streamlines, during the 55-day-long backward integrations starting on the same dates as Fig. 5 (panels **a** to **e**: years 2002 to 2006). The fate of the Lagrangian particles (corresponding to day #0) are the thick BLT areas shown by the *white triangles* in Fig. 5. *Middle and right columns:* same as left column, for depth and salinity of the particles along streamlines, respectively

455 **6 Discussion**

456 Based on the available observations and on a general circulation  
 457 model, we have shown that the BL in the Arabian Sea  
 458 during summer monsoon has a small horizontal extent. It  
 459 appears to be locked on the salinity front separating  
 460 ASHSW and BBW. The model suggests that BL events take  
 461 the form of elongated patterns, stretched along the salinity  
 462 front, with typical length and width of a few hundreds km and  
 463 of 100 km, respectively. This stretched shape can be explained  
 464 by the stirring of the geostrophic current expected to flow  
 465 along the front, as a response to the cross-frontal pressure  
 466 gradient. Because of their spatio-temporal coverage, the avail-  
 467 able observations do not resolve the detailed structure of these  
 468 patterns. As a consequence, the observed summer Arabian Sea  
 469 BL appears as highly porous (with typical porosity of 50 %) at  
 470 the space and time scales resolved for porosity computation  
 471 (2°, 1 month). This corresponds to a space and lifetime of the  
 472 BL of order 15 days and/or 100 km or less.

473 As such, our study contradicts the findings of RS03 and of  
 474 T08, who reported a thick (20 m to over 40 m), large-scale BL  
 475 throughout the central Arabian Sea during summer (July to  
 476 September). The reason for this inconsistency is not straight-  
 477 forward, in particular since T08 used an observational dataset  
 478 similar to ours. To try to find out an explanation for those  
 479 differences in BLT amplitude and surface area (between the  
 480 present study, M09, A12 on one hand and RS03 and T08 on  
 481 the other hand), we perform some tests on the various methods  
 482 used to obtain the final monthly BLT fields. We use the same  
 483 initial dataset for our tests, consisting of all Argo profiles in  
 484 the area between 2004 and 2012 (similar to the dataset used  
 485 for Fig. 2, except that here we do not have Argo before 2004  
 486 nor CTD profiles). For the gridded climatology of T/S profiles  
 487 we use the Roemmich and Gilson (2009) dataset over the  
 488 same period (2004 to 2012), from which we simply obtain  
 489 the T/S profiles annual monthly climatology by averaging the  
 490 9 years (note that our results are nearly identical if we use the  
 491 interannual monthly grids of Roemmich and Gilson (2009)  
 492 instead). We focus on the months of July and August when the  
 493 peak of the BL occurs. Figure 8 shows the final maps of BLT  
 494 for the 2 months, obtained through the three different types of  
 495 methods used in the past and present studies: left column  
 496 shows the resulting monthly maps for a method similar to  
 497 RS03 and A12 (who used a 1 °C BLT criterion from climato-  
 498 logical gridded T and S profiles), middle column shows the  
 499 results for a method similar to T08 (who used a 1 °C BLT

criterion from individual profiles and then performed a map- 500  
 ping through kriging), and right column shows the results of 501  
 the same method similar to T08 except that we use a 0.2 °C 502  
 criterion for BLT (as in the present study). For the central and 503  
 right maps in Fig. 8, the mapping method we chose to get the 504  
 BLT monthly state from individual values uses Data 505  
 Interpolating Variational Analysis (DIVA; Troupin et al. 506  
 2012, with a covariance scale of 4°, and an error of 20 %). It 507  
 is a method very close to optimal interpolation (Troupin et al. 508  
 2012). We also tested a direct ordinary kriging as well as a 509  
 method identical to de Boyer Montégut et al. (2004) and we 510  
 get very similar results (with even slightly less extended 511  
 spatial patterns). 512

We can draw two conclusions from Fig. 8. First, for a given 513  
 BLT criterion (1.0 °C, left and middle columns), computing 514  
 BLT either from individual T/S profiles or from climatological 515  
 T/S grids has not such a strong influence. Resulting patterns 516  
 are similar, with a slightly reduced amplitude for the case of 517  
 BLT based on climatological T/S grids. A reverse effect, i.e., a 518  
 little increase, is seen for the 0.2 °C criterion (not shown), so it 519  
 appears that the bias effect that was discussed for the compu- 520  
 tation of ML depth by de Boyer Montégut et al. (2004) is 521  
 somehow compensated when dealing with a difference of ML 522  
 depths. Second, for a given computation method (BLT based 523  
 of individual T/S profiles, middle and right columns), the 524  
 influence of the criterion on the amplitude of the BLT pattern 525  
 is very minor and does not appear systematic. In July, the 526  
 0.2 °C criterion yields deeper BLTs, while it gives shallower 527  
 BLTs in August. This point will be further discussed in the 528  
 next paragraph. In both months, the 0.2 °C criterion yields a 529  
 BL area of greater extent. 530

By using either a 0.2 °C vs. a 1 °C criterion for the BLT 531  
 computation, we do not pick exactly the same water layer (one 532  
 lies below the other and thus is not exactly associated with a 533  
 BL of identical characteristics, especially its timescales). 534  
 However, on average, the thickness of the layer is not affected 535  
 by the choice of the criterion, at least for our study area. 536  
 Figure 9 provides an example of profiles where the BLT 537  
 obtained through a 0.2 °C criterion can be either larger or 538  
 smaller than the BLT obtained through a 1 °C criterion. This is 539  
 consistent with what is shown in Fig. 8. Note that this result 540  
 might not hold in other areas like the mid or high latitudes 541  
 where the subsurface stratification is much less marked than in 542  
 the tropics (leading to some possible inaccuracies with the 543  
 1 °C criterion). 544

At last, to further clarify the issue of the BL amplitude 545  
 differences, we computed the “revisited-BLT” (in the sense of 546  
 M09). It is defined as the median of all significant BLT in each 547  
 grid cell, calculated after discarding weak BL patterns. It thus 548  
 represents the mean state of BLT when and where a significant 549  
 BL occurs in the grid cell, and not the mean state of the BLT 550  
 over the whole month and area of the grid cell. We obtained a 551  
 value of 20 m to 40 m for summer BLT in the SCAS (not 552



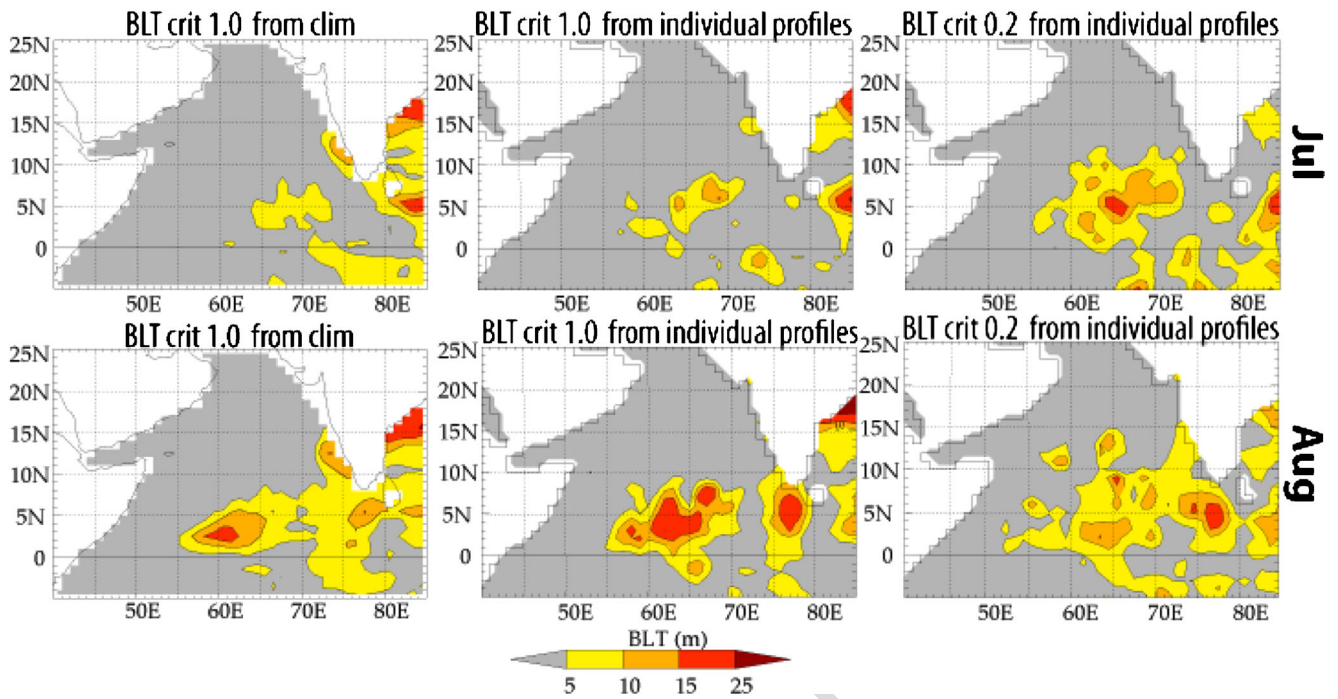
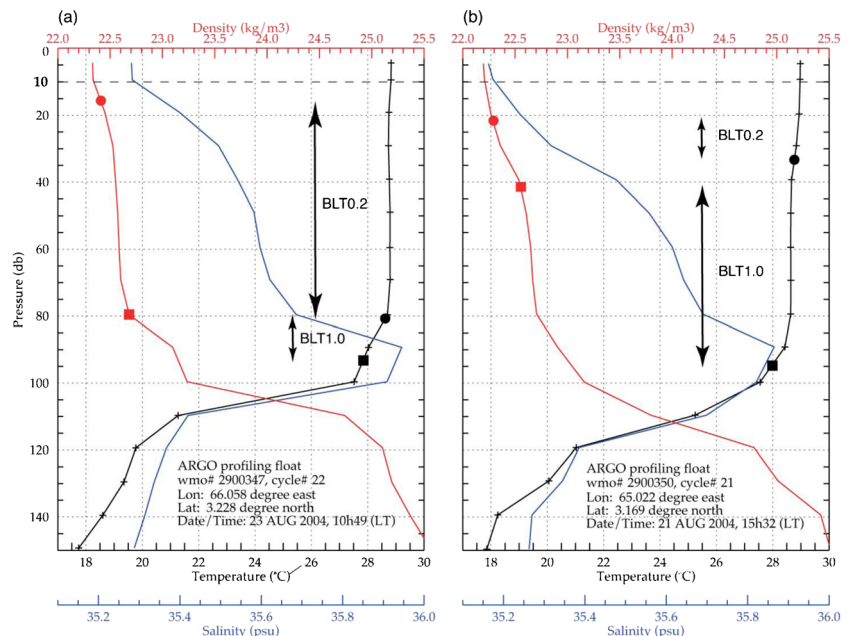


**Fig. 8** Maps of the climatological state of barrier layer thickness (BLT) for the months of July (*top panels*) and August (*bottom panels*), obtained from three different methods: estimation of BLT with a 1 °C criterion from climatological gridded T/S profiles (*left column*), estimation of BLT with a 1 °C criterion from individual profiles and gridding (*middle column*), estimation of BLT with a 0.2 °C criterion from individual profiles and gridding (*right column*), see text for details

553 shown), in line with RS03 and T08 estimates. However, this  
 554 revisited BLT is meaningless if considered independently  
 555 from its associated porosity value. It does not represent the  
 556 “barrier” effect of the BL in the studied area, but rather the  
 557 BLT during effective events. Also it is not the method that T08  
 558 or RS03 described to have used.

The conclusion of this sensitivity test stands in line with the  
 study of A12 who reported a thin BLT of 10–15 m (using a  
 1 °C criterion) during summer in the SCAS, as well as with  
 M09 who estimated a BLT of 10–20 m (using a 0.2 °C  
 criterion). Just like in these studies, our climatological BLT  
 estimate (both observed, Fig. 8 right column, and modeled,

**Fig. 9 a** Same as Fig. 1, with the grey bullet indicating the depth where the temperature is 1.0 °C colder than at 10 m (T10), and the orange bullet indicating the depth of the corresponding density increase. The barrier layer thickness in the sense T10-1.0 °C, named BLT1.0, is defined as the depth difference between the grey and orange bullets. Here, BLT1.0=14 m, i.e., significantly less than BLT0.2 (65 m). **b** Same as a, for another ARGO profile (float # 2900350), in the same area and in the same period (the two stations are separated by 2 days and 115 km). For profile b, we have BLT0.2=12.6 m and BLT1.0=53.5 m (i.e., significantly more than BLT0.2)





565 Fig. 2c) is quite thin (inferior to 25 m) in the SCAS during  
 566 summer, because of the year-to-year variability of the location  
 567 of the isolated events of thick BL discussed above. The ampli-  
 568 tude of the climatological BL reported by RS03 and T08  
 569 exceeds our estimates by a factor of about 2 (extended BLT  
 570 over 40 m in August for T08). We can conclude that this cannot  
 571 be explained by the method used (neither the BLT criterion, nor  
 572 the use of individual T/S profiles vs. climatological T/S grids)  
 573 as we showed above for a given dataset. Thus it appears that  
 574 such a thick BL is doubtful, and we cannot provide any  
 575 explanation about the reason for this inconsistency.

576 In all cases, using objective mapping as a method to fit the  
 577 basic hydrographic data (either T/S profiles, or BLT individual  
 578 values), smoothens the distributions to a significant degree. In  
 579 both our case and T08 study, this creates relatively extended  
 580 spatial patterns of BL. This hides the details, in particular the  
 581 role of the mesoscale fronts evidenced in this work. This may  
 582 explain why T08 describe the BL formation as a large-scale  
 583 process. In the present study, both the use of the porosity index  
 584 and of an OGCM allowed us to infer the short space and time  
 585 scales of the BL events.

586 Our circulation model showed that the formation process of  
 587 summer BL in the SCAS is essentially the tilting mechanism  
 588 defined by Cronin and McPhaden (2002), though with a  
 589 distinctive feature: most of the time, ASHSW gets  
 590 downwelled at the salinity front before flowing beneath  
 591 BBW and building up the BL. As such, the formation mech-  
 592 anism we propose is similar to the one suggested by T08,  
 593 although our model shows that this layered structure is of  
 594 small spatial and temporal extent in the close vicinity of the  
 595 frontal area, and is not seen at large scale as they suggested.  
 596 Interestingly, our study evidences a meso-scale BL formation  
 597 process, capable of generating extremely thick BL patterns  
 598 without any external freshwater supply.

599 That last point holds effectively for the major BL events we  
 600 have chosen in the model to illustrate the role of fronts in their  
 601 formation. However, our area of study (especially the box in  
 602 Fig. 2), while being out of the main monsoon precipitation  
 603 zone, may experience some episodic rainfall events. From  
 604 June to September, climatological monthly values are around  
 605 5 mm/day in that box, and daily precipitation of about 50 mm  
 606 can be observed from TRMM dataset (3b42\_v6 product),  
 607 especially around the southern and eastern edge of the box,  
 608 while north and west are very rarely exposed to precipitations.  
 609 It has been shown that BL can form and last for a day or more  
 610 (depending on the wind conditions) with, for example, rainfall  
 611 events of about 60 mm in 2 h (Price 1979; You 1998), which  
 612 are not represented by our model. As a matter of fact, while the  
 613 frontal mechanism certainly occurs for the majority of thick  
 614 BL events in SCAS, we cannot totally exclude that some  
 615 rainfall mechanism may also happen locally at some occa-  
 616 sions for not more than a few days, especially around southern  
 617 and eastern edge of our box of study.

618 Because of its limited spatial and temporal scales, the  
 619 summertime Arabian Sea BL probably plays a negligible  
 620 climatic role: globally, at large scale, the Arabian Sea can be  
 621 considered as essentially BL-free throughout the summer  
 622 monsoon.

623 The BL formation mechanism we invoke implies an active  
 624 role of the mesoscale circulation in the frontal area. However,  
 625 one has to keep in mind that our model is eddy-permitting  
 626 only, and in particular does not represent the sub-mesoscale  
 627 circulation nor the baroclinic instabilities likely to develop in  
 628 the mixed-layer in the frontal area. It will be necessary to re-  
 629 visit our conclusions with a fully eddy-resolving model of the  
 630 Arabian Sea, when such high-resolution systems become  
 631 available.

**Acknowledgements** This study was funded by IRD, IFREMER,  
 632 MERCATOR-Océan and CNRS. Support from these institutions is grate-  
 633 fully acknowledged. We are indebted to the people who set up the  
 634 International ARGO Project and made the ARGO dataset freely available.  
 635 The model simulations were performed on a SGI computer. We made  
 636 extensive use of the SAXO software (<http://forge.ipsl.jussieu.fr/saxo>)  
 637 developed by Sébastien Masson for plotting. We appreciated  
 638 constructive comments by Gurvan Madec. 639

**References**

640  
 641  
 642 Agarwal N et al (2012) Argo observations of barrier layer in the tropical  
 643 Indian Ocean. *J Adv Space Res*. doi:10.1016/j.asr.2012.05.021  
 644 Antonov JI, Locamini RA, Boyer TP, Mishonov AV, Garcia HE (2006)  
 645 In: Levitus S (ed) World ocean atlas 2005, Volume 2: Salinity.  
 646 NOAA Atlas NESDIS 62, U.S. Government Printing Office,  
 647 Washington, D.C, 182 pp  
 648 Blanke B, Delecluse P (1993) Variability of the tropical Atlantic Ocean  
 649 simulated by a general circulation model with two different mixed  
 650 layer physics. *J Phys Oceanogr* 23:1363–1388  
 651 Blanke B, Raynaud S (1997) Kinematics of the Pacific Equatorial  
 652 Undercurrent: an Eulerian and Lagrangian approach for GCM re-  
 653 sults. *J Phys Oceanogr* 27:1038–1053  
 654 Blanke B, Arhan M, Madec G, Roche S (1999) Warm water paths in the  
 655 equatorial Atlantic as diagnosed with a general circulation model. *J*  
 656 *Phys Oceanogr* 29:2753–2768  
 657 Chatterjee A, Shankar D, Shenoi SSC, Reddy GV, Michael GS,  
 658 Ravichandran M, Gopalakrishna VV, Rama Rao EP, Udaya  
 659 Bhaskar TVS, Sanjeevan VN (2012) A new atlas of temperature  
 660 and salinity for the North Indian Ocean. *J Earth Syst Sci* 121(3):  
 661 559–593  
 662 Cronin MF, McPhaden MJ (2002) Barrier layer formation during west-  
 663 erly wind bursts. *J Geophys Res* 107(C12):8020. doi:10.1029/  
 664 2001JC001171  
 665 de Boyer Montégut C, Madec G, Fischer AS, Lazar A, Iudicone D (2004)  
 666 Mixed layer depth over the global ocean: an examination of profile  
 667 data and a profile-based climatology. *J Geophys Res* 109, C12003.  
 668 doi:10.1029/2004JC002378  
 669 de Boyer Montégut C, Mignot J, Lazar A, Cravatte S (2007a) Control of  
 670 salinity on the mixed layer depth in the world ocean: 1. General  
 671 description. *J Geophys Res* 112(C06011)  
 672 de Boyer Montégut C, Vialard J, Shenoi SSC, Shankar D, Durand F, Ethé  
 673 C, Madec G (2007b) Simulated seasonal and interannual variability

674 of mixed layer heat budget in the north Indian Ocean. *J Clim* 20: 708  
 675 3249–3268 709

676 Durand F, Shankar D, de Boyer Montégut C, Shenoi SSC, Blanke B, 710  
 677 Madec G (2007) Modeling the barrier-layer formation in the South- 711  
 678 Eastern Arabian Sea. *J Clim* 20(10):2109–2120 712

679 Durand F, Alory G, Dussin R, Reul N (2013) SMOS reveals the signature 713  
 680 of Indian Ocean Dipole events. *Ocean Dyn*. doi:10.1007/s10236- 714  
 681 013-0660-y 715

682 Esenkov OE, Olson DB, Bleck R (2003) A study of the circulation and 716  
 683 salinity budget of the Arabian Sea with an isopycnic coordinate 717  
 684 ocean model. *Deep-Sea Res II* 50:2091–2110 718

685 Goosse H, Campin JM, Deleersnijder E, Fichefet T, Mathieu PP, 719  
 686 Maqueda AAM, Tartinville B (2001) Description of the CLIO 720  
 687 model version 3.0. Institut d’Astronomie et de Géophysique 721  
 688 Georges Lemaitre, Catholic University of Louvain, Belgium 722

689 Hoyos CD, Webster PJ (2007) The role of intraseasonal variability in the 723  
 690 nature of Asian monsoon precipitation. *J Clim* 20(17):4402–4424 724

691 Locarnini RA, Mishonov AV, Antonov JI, Boyer TP, Garcia HE (2006) 725  
 692 In: Levitus S (ed) *World ocean atlas 2005, Volume 1: Temperature*. 726  
 693 NOAA Atlas NESDIS 61, U.S. Government Printing Office, 727  
 694 Washington, D.C, 182 pp 728

695 Lukas R, Lindstrom E (1991) The mixed layer of the western equatorial 729  
 696 Pacific Ocean. *J Geophys Res* 96(Suppl):3343–3358 730

697 Madec G (2008) NEMO reference manual, ocean dynamics component. 731  
 698 Note du pôle de modélisation, IPSL France N°27 ISSN N°1288-1619 732

699 Maes C, Picaut J, Belamari S (2005) Importance of salinity barrier layer 733  
 700 for the buildup of El Niño. *J Clim* 18:104–118 734

701 Masson S, Luo JJ, Madec G, Vialard J, Durand F, Gualdi S, Guilyardi E, 735  
 702 Behera S, Delecluse P, Navarra A, Yamagata T (2005) Impact of barrier 736  
 703 layer on winter–spring variability of the South-Eastern Arabian Sea. 737  
 704 *Geophys Res Lett* 32, L07703. doi:10.1029/2004GL021980 738

705 Mignot J, de Boyer Montégut C, Lazar A, Cravatte S (2007) Control of 739  
 706 salinity on the mixed layer depth in the world ocean: 2. Tropical 740  
 707 areas. *J Geophys Res* 112, C10010. doi:10.1029/2006JC003954 741  
 742

Mignot J, de Boyer Montégut C, Tomczak M (2009) On the porosity of 708  
 barrier layers. *Ocean Sci* 5:379–387 709

Prasad TG, Ikeda M (2002) A numerical study of the seasonal variability 710  
 of Arabian Sea high-salinity water. *J Geophys Res* 107(C11):3197. 711  
 doi:10.1029/2001JC001139 712

Prasanna Kumar S, Prasad TG (1999) Formation and spreading of 713  
 Arabian Sea high salinity water mass. *J Geophys Res* 104(C1): 714  
 1455–1464 715

Price JF (1979) Observations of a rain-formed mixed layer. *J Phys 716  
 Oceanogr* 9:643–649 717

Rao RR, Sivakumar R (2003) Seasonal variability of sea surface salinity 718  
 and salt budget of the mixed layer of the north Indian Ocean. *J 719  
 Geophys Res* 108:3009. doi:10.1029/2001JC000907 720

Roemmich D, Gilson J (2009) The 2004–2008 mean and annual cycle of 721  
 temperature, salinity, and steric height in the global ocean from the 722  
 Argo Program. *Progr Oceanogr* 82:81–100 723

Thadathil P, Thoppil P, Rao RR, Muraleedharan PM, Somayaju YK, 724  
 Gopalakrishna VV, Murthugudde R, Reddy GV, Revichandran C 725  
 (2008) Seasonal variability of the observed barrier layer in the 726  
 Arabian Sea. *J Phys Oceanogr* 38:624–638 727

Tomczak M (1999) Some historical, theoretical and applied aspects of 728  
 quantitative water mass analysis. *J Mar Res* 57:275–303 729

Troupin C, Barth A, Sirjacobs D, Ouberdous M, Brankart J-M, Brasseur 730  
 P, Rixen M, Alvera Azcarate A, Belounis M, Capet A, Lenartz F, 731  
 Toussaint M-E, Beckers J-M (2012) Generation of analysis and 732  
 consistent error fields using the Data Interpolating Variational 733  
 Analysis (Diva). *Ocean Model* 52–53:90–101 734

Vialard J, Delecluse P (1998) An OGCM study for the TOGA decade: 735  
 part II. Barrier layer formation and variability. *J Phys Oceanogr* 28: 736  
 1089–1106 737

Wirth A, Willebrand J, Schott F (2002) Variability of the Great Whirl 738  
 from observations and models. *Deep-Sea Res II* 49:1279–1295 739

You Y (1998) Rain-formed barrier layer of the western equatorial Pacific 740  
 warmpool: a case study. *J Geophys Res* 103(C3):5361–5378 741

## AUTHOR QUERIES

### **AUTHOR PLEASE ANSWER ALL QUERIES.**

- Q1. Please check if the affiliations are captured and presented correctly.
- Q2. “Arakawa (1966)” is cited in text but not given in the reference list. Please provide details in the list or delete the citation from the text.
- Q3. The citation “Locarnini et al. 2005” (original) has been changed to “Locarnini et al. 2006”. Please check if appropriate.
- Q4. The citation “Durand et al. (2008)” (original) has been changed to “Durand et al. (2007)”. Please check if appropriate.
- Q5. Please define OGCM.

UNCORRECTED PROOF